Marine Geodesy, Volume 18, pp. 139–156
Printed in the UK.

0149-0419/95 $10.00 + .00

Role of Water Vapor Radiometers for In-Flight Calibration of the TOPEX Microwave Radiometer

STEPHEN J. KEIHM

Jet Propulsion Laboratory
California Institute of Technology
Pasadena, California, USA

CHRISTOPHER S. RUF

Department of Electrical Engineering
The Pennsylvania State University
University Park, Pennsylvania, USA

First-year results are presented for the in-flight calibration and performance evaluation of the TOPEX microwave radiometer (TMR) based on overflight comparisons with ground-based water vapor radiometer (WVR) data. Comparisons are made in terms of both TMR brightness temperatures and the retrieved range correction due to tropospheric water vapor (path delay).

Comparisons of TMR brightness temperature measurements with predictions based on WVR data and a calm sea flux model provided early recognition of TMR preflight calibration errors which were not apparent based on ground truth path delay comparisons. Later comparisons, using the final TMR calibration algorithms, are used to constrain the model for the calm sea surface nadir emissivity. The results suggest that the 18- to 37-GHz calm sea flux is enhanced 1–2 K relative to the predictions of a Fresnel model for a plane surface.

Comparisons in the path delay domain illustrate the advantages of using time and space coincident ground measurements for in-flight calibration and performance monitoring of satellite radiometer measurements. The results demonstrate that elimination of temporal and spatial decorrelation errors reduces path delay comparison

The authors acknowledge several individuals and organizations for their assistance with this work. Peter Gaiser and Karen St. Germaine of the University of Massachusetts deployed and operated the WVRs at Chichi Jima and Norfolk. The Japanese Local Meteorological Observatories and the Australian Bureau of Meteorology were very helpful in facilitating the WVR deployments at Chichi Jima and Norfolk. Robert Jablonski and Philip de Blieck, under the authority of Commander L.T.J.G. Catalano at the U.S. Coast Guard station at Lampedusa, monitored the performance of the Lampedusa WVR and provided timely data transfers throughout the first year of operation. Alan Tanner of the Jet Propulsion Laboratory maintained the WVRs at Harvest and Lampedusa.

This work presents the results of one phase of research conducted at the Jet Propulsion Laboratory, California Institute of Technology, Pasadena, under contract to the National Aeronautics and Space Administration.

Address correspondence to Dr. Stephen J. Keihm, M/S 246-101, Jet Propulsion Laboratory, Pasadena, CA 91109, USA.

residuals to less than 1 cm, in contrast to the 3-cm scatter produced by the customary radiosonde comparisons.

Keywords TOPEX microwave radiometer, water vapor radiometer, wet troposphere range correction, path delay, in-flight calibration, brightness temperature.

Altimetry measurements of sea level require a number of corrections for atmosphere-induced time delays, one of which is that caused by tropospheric water vapor and cloud liquid. This delay, expressed as a range correction (hereafter referred to as path delay), is highly variable in time and space, ranging from ~3 cm for cold, dry conditions to 45 cm for warm, humid conditions. The TOPEX microwave radiometer (TMR) was included in the TOPEX/Poseidon altimetry mission to provide the path delay correction to an accuracy of 1.2 cm (Carlisle et al., 1991). The TMR consists of three nadir-viewing channels (18, 21, and 37 GHz) which measure the emission (brightness temperature) from the atmosphere and sea surface. The 21-GHz channel, operating near the peak of the 22.235-GHz water vapor absorption resonance, is the primary vapor-sensing channel. The 37-GHz channel is most sensitive to liquid water and provides a measurement used to separate the liquid and vapor contributions in the presence of clouds. The 18-GHz channel provides a correction for variability in the sea surface background flux due mainly to the effects of wind on the surface emissivity. Due to the frequency proximity of the 18- and 21-GHz channels, they respond nearly equally to variations in the sea surface flux. Thus, variations in atmospheric water vapor abundance, and the related path delay, are strongly correlated with the brightness temperature difference between the 21- and 18-GHz measurements. For further details on the interpretation of the TMR measurements in terms of path delay (the ''retrieval algorithm''), see Keihm et al. (1995).

In-flight calibration of the TMR antenna temperature measurements is performed by alternately switching the radiometer input between the main antenna, a smaller antenna pointed into cold space, or to an internal matched load. The antenna temperature calibration equations take into account hardware component losses and their temperature dependencies, which were determined prior to launch in a series of thermal vacuum (T/V) tests (Ruf et al., 1995). Error sources associated with the prelaunch antenna temperature algorithm include errors in the extrapolation from T/V-simulated cold space at ~77 K to in-flight cold space at ~2.7 K, high-order instrument nonlinearities not properly modeled by the quadratic calibration algorithm, and small measurement errors in the T/V tests.

The conversion of antenna temperatures to nadir brightness temperatures requires a second calibration algorithm which takes into account side lobe contributions to the measured signals (Janssen et al., 1995). Antenna range measurements, conducted prior to launch, were used to determine beam pattern parameters which were included in the antenna pattern correction (APC) algorithm. Error sources associated with the APC include errors in the antenna range measurements and uncertainties in the brightness temperatures viewed by the on-Earth side lobes. An additional potential source of APC algorithm error was a last-minute thermal blanketing modification to the antenna, made prior to launch but after the antenna range measurements were completed (Ruf et al., 1995).

In-flight testing of the TMR calibration algorithms was carried out during the 6-month verification phase following launch. Various sources of ''ground truth,'' including radiosondes, water vapor radiometers (WVRs), and climatological models, were compared with overflown TMR measurements in both the brightness temperature and retrieved path delay domains. Similar to verification studies for previously flown water vapor

microwave sensors (e.g., Lipes, 1982; Alishouse et al., 1990), radiosondes were used as the primary calibration standard in the integrated water vapor (path delay) domain (Ruf et al., 1995). Twenty-three island radiosonde launch sites, located within 50 km of the TOPEX/Poseidon groundtrack, were used as the comparison database. Radiosondes offer three primary advantages for calibration of water vapor–related satellite measurements: no-cost availability, abundance of data, and direct measurement of the vapor and temperature profiles which determine the path delay. The primary disadvantages are large temporal and spatial decorrelations relative to the TMR measurements and errors in the radiosonde relative humidity measurements, especially in the presence of clouds or very dry conditions (Schwartz and Doswell, 1991). In addition, comparisons in the path delay domain alone do not reveal the source(s) of in-flight calibration errors. As demonstrated by the early TMR performance and described in this paper, satisfactory comparisons can be obtained in the path delay domain while large, but compensating, errors are present in the satellite brightness temperature measurements.

Ground-based WVRs are especially useful for satellite microwave sensor calibration in the brightness temperature domain. WVRs directly measure the atmospheric emissions, which are the main source of variability in the open ocean satellite microwave measurements. To predict TMR brightness temperatures from the WVR measurements, a sea surface flux model is required to account for the background contributions to the nadir viewing measurements. For calm conditions this model is well constrained (within an accuracy of a few degrees Kelvin) by knowledge of the sea surface temperature. In fact, results of the final TMR algorithm adjustments suggest that the TMR operational brightness temperature accuracies are sufficient to refine the calm ocean model flux levels at the TMR frequencies to accuracies of 1–2 K.

In this paper the role of WVRs in the TMR in-flight calibration is emphasized. In the next section we describe the deployment and operational characteristics of the WVRs used in the TMR verification processing. The following section presents results of TMR–WVR comparisons in the brightness temperature domain. Data which led to the early detection of large TMR antenna calibration errors are shown, followed by the results of the first year of comparisons using the final TMR calibration algorithms. In this section evidence is presented suggesting that the actual calm sea flux is enhanced 1–2 K above the Fresnel predictions for a flat surface. The next section presents TMR–WVR comparisons in the path delay domain based on the final TMR algorithms and the first year of data. In the last section the WVR comparison results are summarized and lessons learned regarding the utilization of WVRs for satellite instrument calibration are discussed.

WVR Deployment and Operation

For the purposes of validation of the altimeter and TMR performance, WVRs were deployed prior to cycle 1 measurements, and have continued operation, at Lampedusa Island (35.57N, 12.57E), in the Mediterranean Sea, and the Harvest oil platform (34.47N, 120.68W), 11 km from California coastline near Santa Barbara. These were the primary verification sites for the Poseidon (CNES) and TOPEX (NASA) altimeters, respectively. The verification site WVRs are identical three-frequency J units, built at the Jet Propulsion Laboratory, with channels at 20.7, 22.2, and 31.4 GHz. In addition, a JPL D unit WVR, operating at 20.7 and 31.4 GHz, was deployed for ~1-month periods at the island sites of Chichi Jima, Japan (27.08N, 142.18E) during September 1992, and Norfolk, Australia (29.03S, 167.93E) during October 15–November 15, 1992. These sites were chosen for their proximity to the TOPEX/Poseidon groundtrack and to provide high (Chichi Jima)

and low (Norfolk) end humidity condition comparisons early in the verification phase. Minimum groundtrack separations at the four WVR sites are 21 km at Lampedusa, 0 km at Harvest (direct overflight), 32 km at Chichi Jima, and 29 km at Norfolk.

At all sites the WVRs operated in a continuous tipping curve mode, monitoring instrument gain and zenith sky brightness temperature variations at a 1.5-min sampling rate. In this mode absolute brightness temperature accuracies of 0.5 K have been demonstrated for the J- and D-unit radiometers (Keihm, 1991). The zenith measurements were converted to integrated vapor abundance and path delay using statistical retrievals based on correlations with computed brightness temperatures from radiosonde data archives. The uncertainty in WVR-retrieved path delay is less than 0.3 cm due to instrument effects alone. The largest error in the path delay retrieval is due to a ~5–10% uncertainty in the line strength of the vapor absorption model required to convert the measured brightness temperatures to vapor abundance (path delay). Since the same model of vapor absorption was used in both the TMR and WVR path delay retrieval algorithms (Keihm et al., 1994a), this error is transparent for TMR–WVR comparisons in the path delay domain.

In the brightness temperature domain, the TMR–WVR comparisons are unaffected by the absorption model line strength uncertainty since both instruments provide direct measurements of the atmospheric emission. Comparisons of TMR with WVR predictions do require a conversion of the WVR measurements to the TMR frequencies and a model for the sea surface flux contribution to the downward-viewing TMR. The frequency conversion produces negligible error because the vapor absorption model line shape is well constrained (Hill, 1986; Keihm, 1992). For the sea surface flux component, measured sea surface temperatures were multiplied by temperature-dependent Fresnel emissivities calculated from the Klein and Swift (1977) formulation for ocean dielectric properties. For the brightness temperature domain comparisons, only calm sea TMR data, as determined from the TMR wind speed algorithm (Keihm et al., 1995), was used to minimize emissivity variations due to wind-generated foam and roughness. The complete algorithm used to convert WVR brightness temperatures to predicted TMR brightness temperatures is presented by Ruf et al. (1994).

Through August 1993, ~100 overflight comparisons of the WVR sites have been obtained, including 12 from the temporary stations at Chichi Jima and Norfolk. At Lampedusa, where both ascending and descending groundtracks lie within 50 km of the site, 55 TMR–WVR comparisons were obtained over the first year of operation. No Lampedusa WVR data were obtained over a 6-week interval at the end of 1992 due to a hardware failure incurred during a severe electrical storm. At the Harvest oil platform numerous WVR hardware failures occurred, resulting in the loss of 12 of the first 40 cycles of overpass comparison data. These failures can be attributed to the harsh environmental conditions at Harvest. In addition to the salt sea air effects, the Harvest WVR is located less than 4 m from a helicopter landing pad and is subject to intense vibrations four times daily during the helicopter landings and takeoffs.

Results of TMR–WVR Brightness Temperature Comparisons

Early Detection of TMR Brightness Temperature Offsets

Within 6 weeks postlaunch, prior to the completion of orbit maneuvers and the onset of cycle 1 data, Harvest and Lampedusa overflight comparisons of TMR- and WVR-pre-

dicted brightness temperatures revealed 6- to 12-K offsets, with the TMR low in all channels (Figure 1, open squares). The problem was not apparent in the path delay domain comparisons because the offsets produced largely compensating effects in the path delay retrieval algorithm. (Recall that the TMR-derived retrievals are strongly correlated with the 21 − 18 GHz brightness temperature differences.) To determine the source of the large offsets, a number of possible explanations were considered, including errors in the APC algorithm, errors in our assumed model of sea surface flux, and errors in the antenna temperature calibration. After eliminating the APC and surface flux model uncertainties as insufficient to produce the observed offsets, we discovered that part of the prelaunch T/V data, used to calibrate the TMR sensitivity to the cold sky brightness temperature, was invalid due to large temperature gradients present in the T/V cold sky target. The error was corrected by identifying other T/V data taken when the cold sky target temperature was stable. The resultant revised antenna temperature calibration algorithm essentially removed all of the biases relative to the WVR comparison data (cross data of Figure 1).

The results shown in Figure 1, based on the revised antenna temperature algorithm, do not represent the final TMR brightness temperature calibration. Smaller adjustments were later required based primarily on the TMR–radiosonde comparisons in the path delay domain. These comparisons revealed a scale error of ~10%, after the antenna temperature calibration revision, with the TMR-derived path delays increasingly low relative to the radiosonde measurements for moderate to high vapor conditions. The scale error was corrected by refinements to both the APC algorithm and the vapor absorption model line strength used in the path delay retrieval algorithm. The division of the correction was based on a number of considerations:

1. Using the preflight APC algorithm, comparisons of the TMR brightness temperatures with data from the special sensor microwave/imager (SSM/I) radiometer over the Amazon rain forest revealed biases of 6–9 K (TMR low) for the highest brightness temperatures measured, where gain errors have the largest effect. The nadir-viewing TMR brightness temperatures were predicted from the 53° slant angle SSM/I measurements by including only SSM/I data for which the vertical and horizontal polarization channel differences were less than 1 K. Model calculations demonstrate that nadir brightness temperatures should be within 3 K and below the SSM/I measurements when the <1 K polarization criterion occurs. This result is insensitive to plausible uncertainties in land temperature, surface roughness, and atmospheric opacity. Ruf et al. (1994) provide details of the TMR-SSM/I comparisons.
2. Using the preflight APC algorithm, the TMR–WVR path delay comparisons were consistent with a smaller scale error, ~5%, although the number and range of the early comparisons were insufficient to constrain the scale error by better than a factor of 2. This result suggested that at least part of the scale error was due to instrument calibration effects, since the TMR–WVR path delay comparisons are transparent to absorption model errors.
3. A downward adjustment of the vapor absorption model line strength by more than 5% would be inconsistent with both the only available laboratory measurements (Becker and Autler, 1946) and radiosonde–WVR intercomparison results (Keihm, 1992).

Based on the above considerations, the 10% path delay scale error in the TMR–radiosonde comparisons was eliminated by a combination of ~5% gain increases in the

APC algorithm for the three TMR channels and a 5% reduction in the vapor absorption model line strength parameter used in the retrieval algorithm. The APC adjustment produced agreement between the SSM/I-predicted and TMR-measured brightness temperatures for the Amazon rain forest data. The APC adjustment also eliminated the ~5% scale error in the TMR–WVR path delay comparisons. The vapor absorption model adjustment had no effect on the TMR–WVR path delay comparisons because the same adjustment was applied to both the TMR and WVR path delay retrieval algorithms. For a more detailed discussion of the final TMR algorithm modifications, see Ruf et al. (1994).

TMR–WVR Brightness Temperature Comparisons Using the Final TMR Calibration Algorithms

The final TMR instrument gain adjustments have been used to recompute the TMR-measured vs. WVR-predicted brightness temperature comparisons over the first full year of operation. The results, shown in Figure 2 for the Harvest, Lampedusa, and Norfolk sites, include only overpasses characterized by low wind speeds and cloud-free conditions. The Chichi Jima results are not shown because only two of the overpasses satisfied the clear, calm criteria.

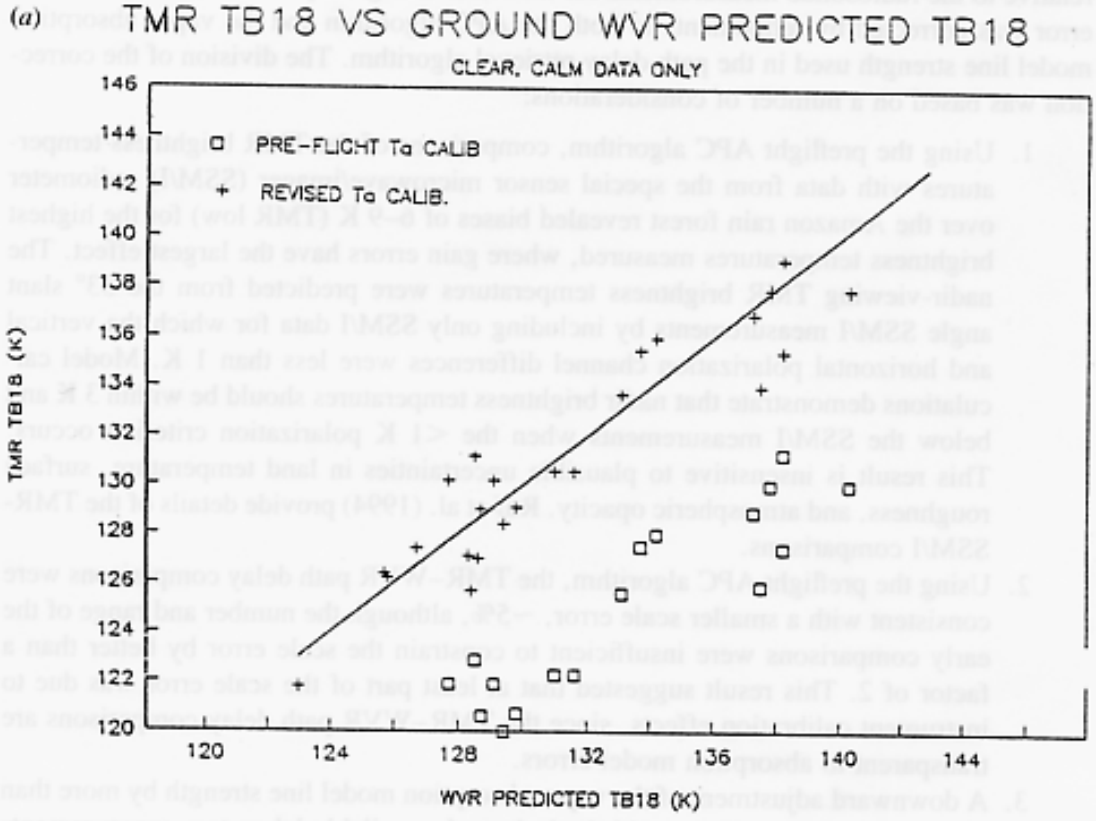

Figure 1. Pre–cycle 1 comparisons of measured and WVR-predicted TMR brightness temperatures at 18 (a), 21 (b), and 37 GHz (c) from the Harvest and Lampedusa verification sites. The 6- to 12-K TMR offsets were effectively removed when postlaunch corrections to the antenna temperature calibration algorithm were applied. The final modifications to the TMR antenna pattern algorithm have not yet been implemented.

(*b*)

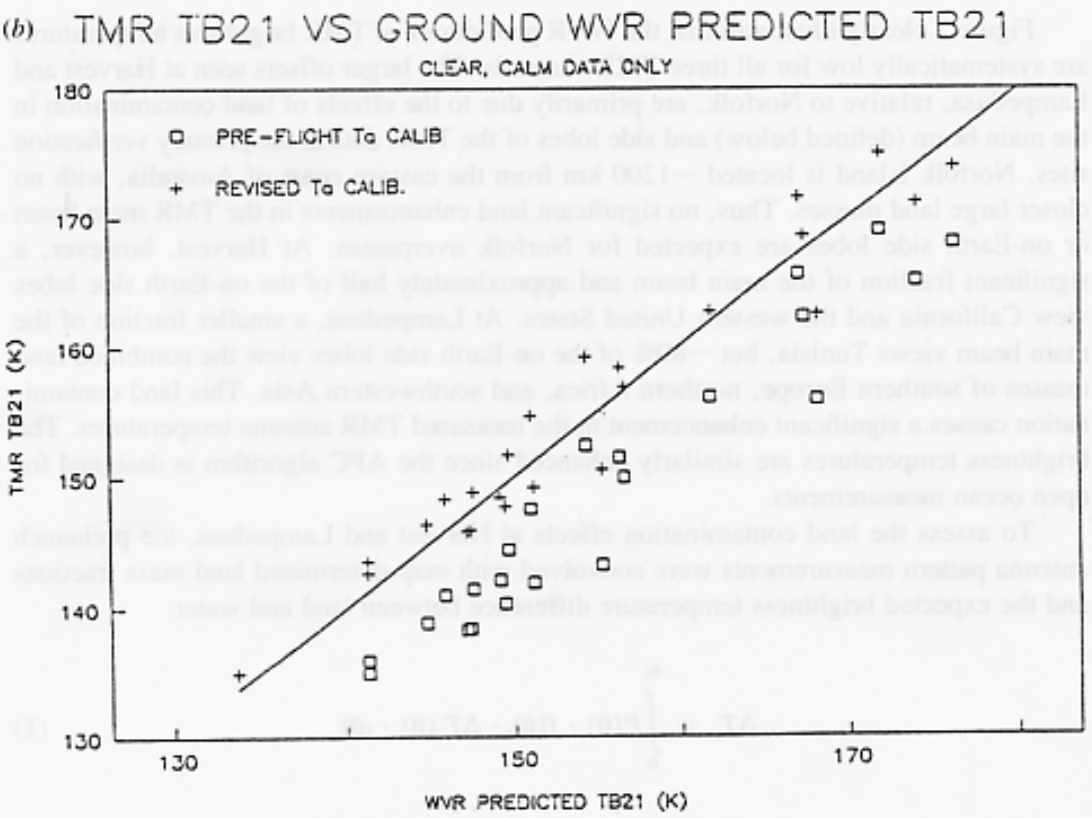

(*c*)

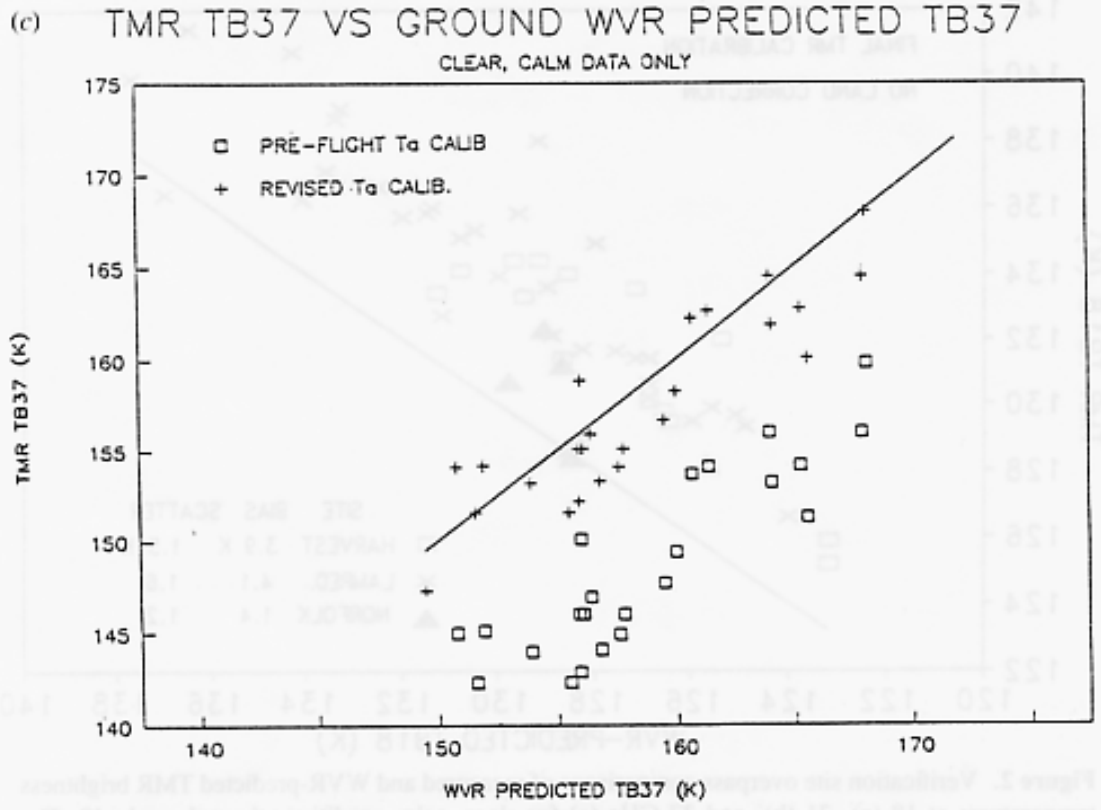

Figure 1. (*Continued*)

Figure 2 clearly illustrates that the WVR predictions of TMR brightness temperatures are systematically low for all three TMR channels. The larger offsets seen at Harvest and Lampedusa, relative to Norfolk, are primarily due to the effects of land contamination in the main beam (defined below) and side lobes of the TMR data at the primary verification sites. Norfolk Island is located ~1200 km from the eastern coast of Australia, with no closer large land masses. Thus, no significant land enhancements in the TMR main beam or on-Earth side lobes are expected for Norfolk overpasses. At Harvest, however, a significant fraction of the main beam and approximately half of the on-Earth side lobes view California and the western United States. At Lampedusa, a smaller fraction of the main beam views Tunisia, but ~80% of the on-Earth side lobes view the combined land masses of southern Europe, northern Africa, and southwestern Asia. This land contamination causes a significant enhancement in the measured TMR antenna temperatures. The brightness temperatures are similarly enhanced since the APC algorithm is designed for open ocean measurements.

To assess the land contamination effects at Harvest and Lampedusa, the prelaunch antenna pattern measurements were convolved with map-determined land mass fractions and the expected brightness temperature difference between land and water.

$$\Delta T_a = \int_0^{\theta_L} P(\theta) \cdot f(\theta) \cdot \Delta T_b(\theta) \cdot d\theta \tag{1}$$

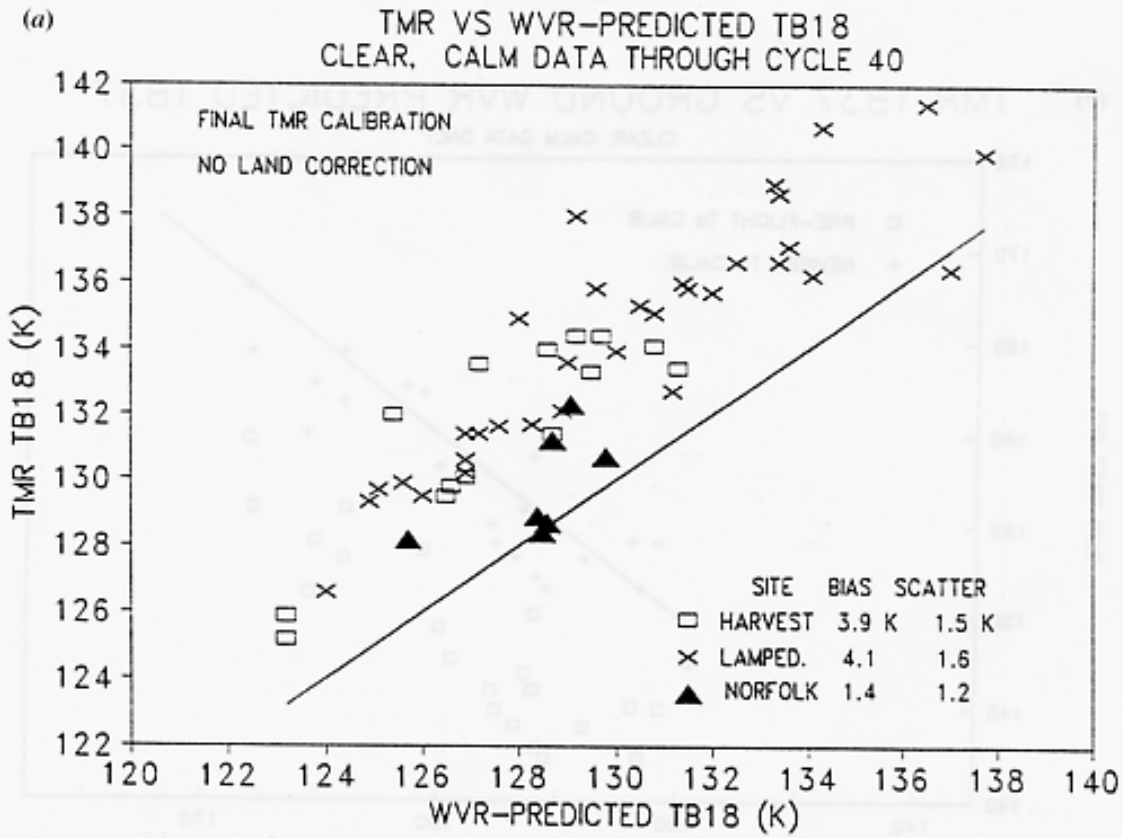

Figure 2. Verification site overpass comparisons of measured and WVR-predicted TMR brightness temperatures at 18 (a), 21 (b), and 37 GHz (c) for clear, calm conditions through cycle 40. The final TMR calibration algorithms have been utilized, but no corrections for land contamination have been applied.

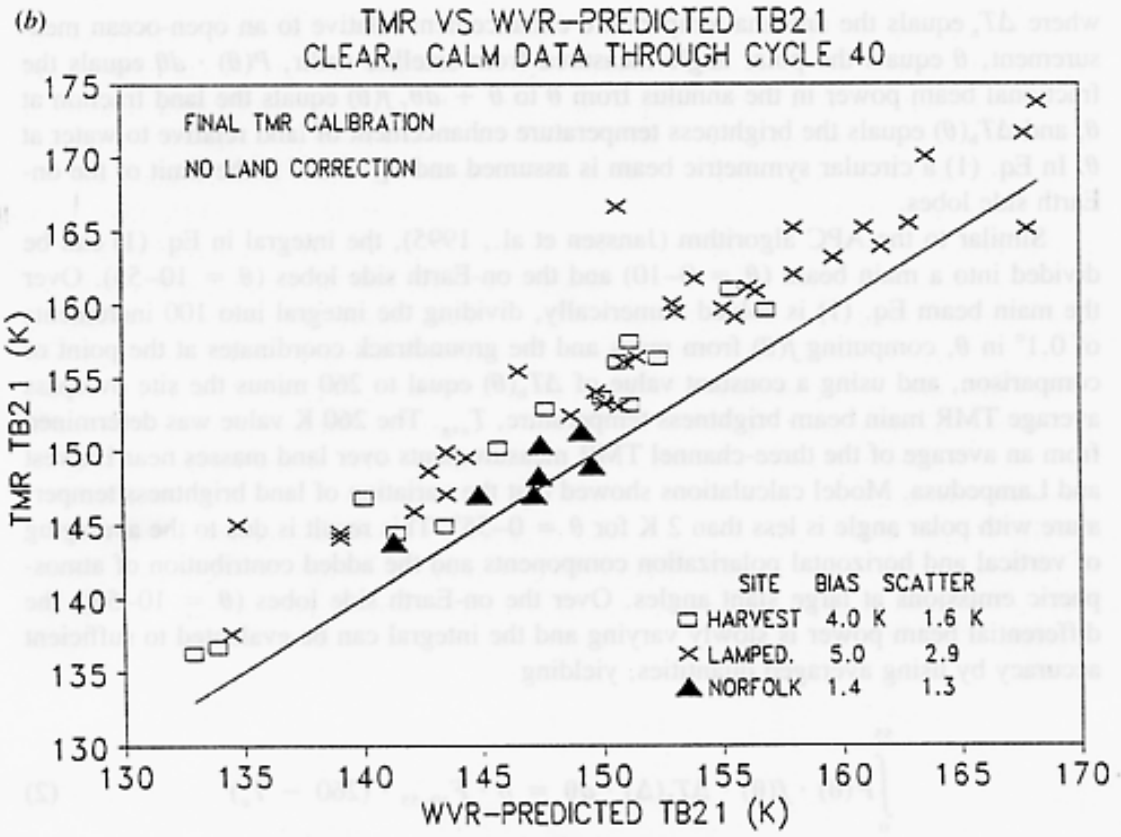

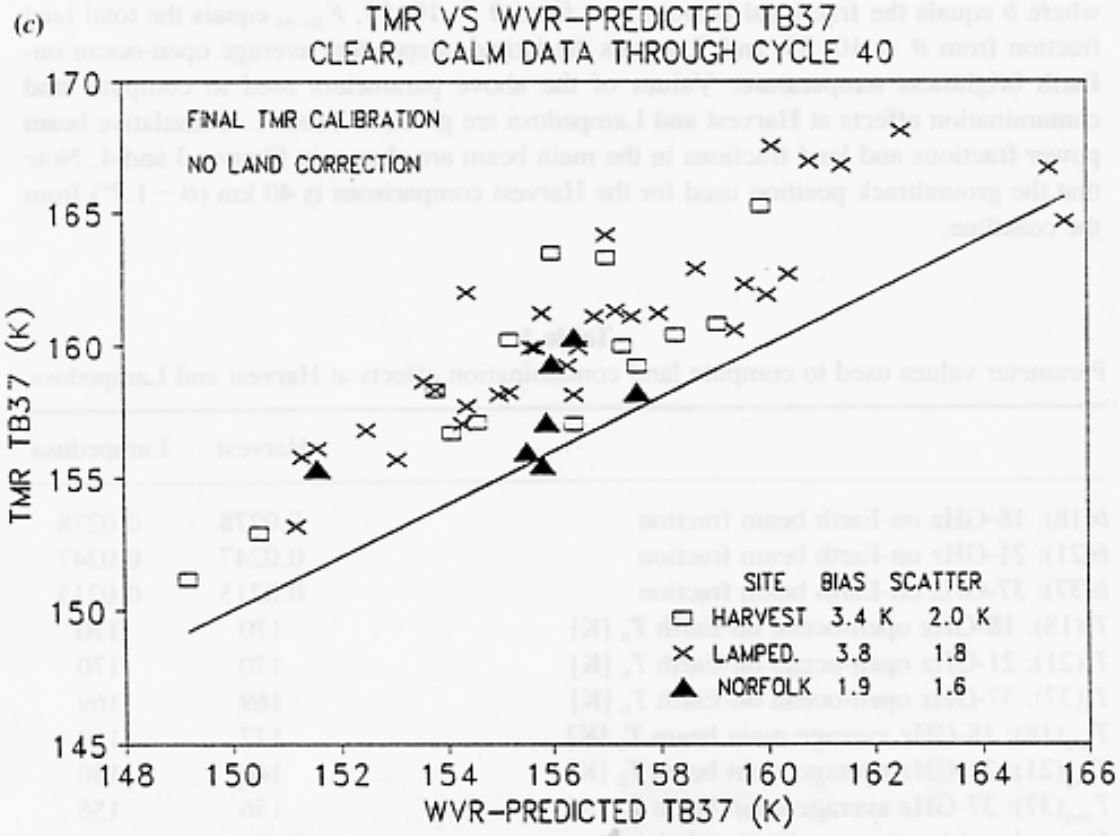

Figure 2. (*Continued*)

where ΔT_a equals the antenna temperature enhancement relative to an open-ocean measurement, θ equals the polar angle measured from satellite nadir, $P(\theta) \cdot d\theta$ equals the fractional beam power in the annulus from θ to $\theta + d\theta$, $f(\theta)$ equals the land fraction at θ, and $\Delta T_b(\theta)$ equals the brightness temperature enhancement of land relative to water at θ. In Eq. (1) a circular symmetric beam is assumed and $\theta_L = 55°$ is the limit of the on-Earth side lobes.

Similar to the APC algorithm (Janssen et al., 1995), the integral in Eq. (1) can be divided into a main beam (θ = 0–10) and the on-Earth side lobes (θ = 10–55). Over the main beam Eq. (1) is solved numerically, dividing the integral into 100 increments of 0.1° in θ, computing $f(\theta)$ from maps and the groundtrack coordinates at the point of comparison, and using a constant value of $\Delta T_b(\theta)$ equal to 260 minus the site overpass average TMR main beam brightness temperature, T_{avg}. The 260 K value was determined from an average of the three-channel TMR measurements over land masses near Harvest and Lampedusa. Model calculations showed that the variation of land brightness temperature with polar angle is less than 2 K for θ = 0–55°. This result is due to the averaging of vertical and horizontal polarization components and the added contribution of atmospheric emissions at large slant angles. Over the on-Earth side lobes (θ = 10–55), the differential beam power is slowly varying and the integral can be evaluated to sufficient accuracy by using averaged quantities, yielding

$$\int_0^{55} P(\theta) \cdot f(\theta) \cdot \Delta T_b(\Delta) \cdot d\theta = b \cdot F_{10-55} \cdot (260 - T_e) \tag{2}$$

where b equals the fractional beam power from θ = 10–55, F_{10-55} equals the total land fraction from θ = 10–55, and T_e equals the latitude-dependent average open-ocean on-Earth brightness temperature. Values of the above parameters used to compute land contamination effects at Harvest and Lampedusa are given in Table 1. Cumulative beam power fractions and land fractions in the main beam are shown in Figures 3 and 4. Note that the groundtrack position used for the Harvest comparisons is 40 km ($\theta \sim 1.7°$) from the coastline.

Table 1
Parameter values used to compute land contamination effects at Harvest and Lampedusa

	Harvest	Lampedusa
b(18): 18-GHz on-Earth beam fraction	0.0278	0.0278
b(21): 21-GHz on-Earth beam fraction	0.0247	0.0247
b(37): 37-GHz on-Earth beam fraction	0.0215	0.0215
T_e(18): 18-GHz open-ocean on-Earth T_b [K]	170	170
T_e(21): 21-GHz open-ocean on-Earth T_b [K]	170	170
T_e(37): 37-GHz open-ocean on-Earth T_b [K]	169	169
T_{avg}(18): 18-GHz average main beam T_b [K]	127	130
T_{avg}(21): 21-GHz average main beam T_b [K]	146	150
T_{avg}(37): 37-GHz average main beam T_b [K]	156	156
F_{10-55}: Land fraction, on-Earth side lobes	0.48	0.80

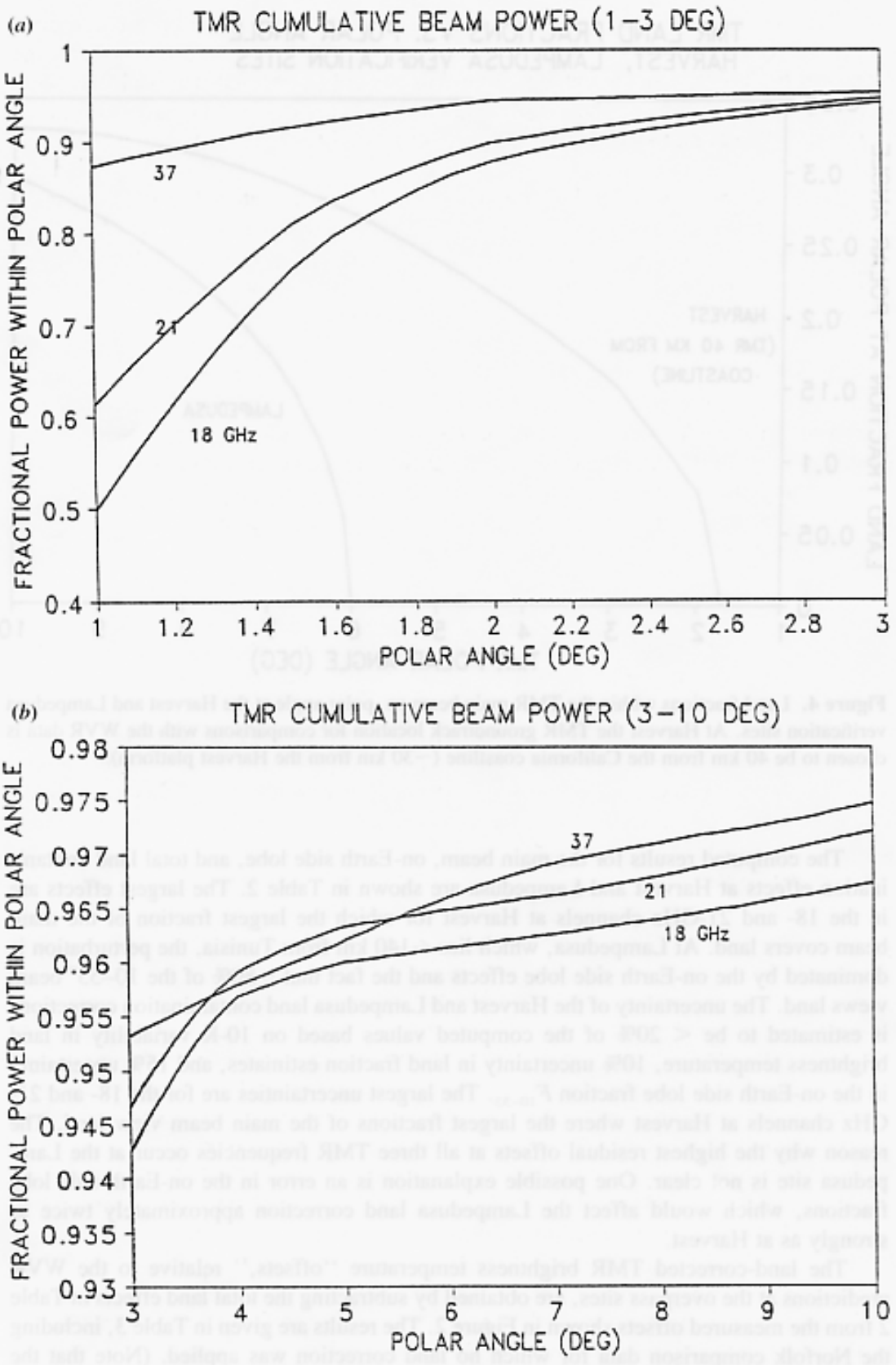

Figure 3. Cumulative TMR beam power as a function of polar angle for θ = 1–3° (a) and 3–10° (b) as determined from prelaunch antenna pattern measurements. Within the main beam (θ = 0–10°) each degree of polar angle corresponds to ~23.3 km along the Earth's surface.

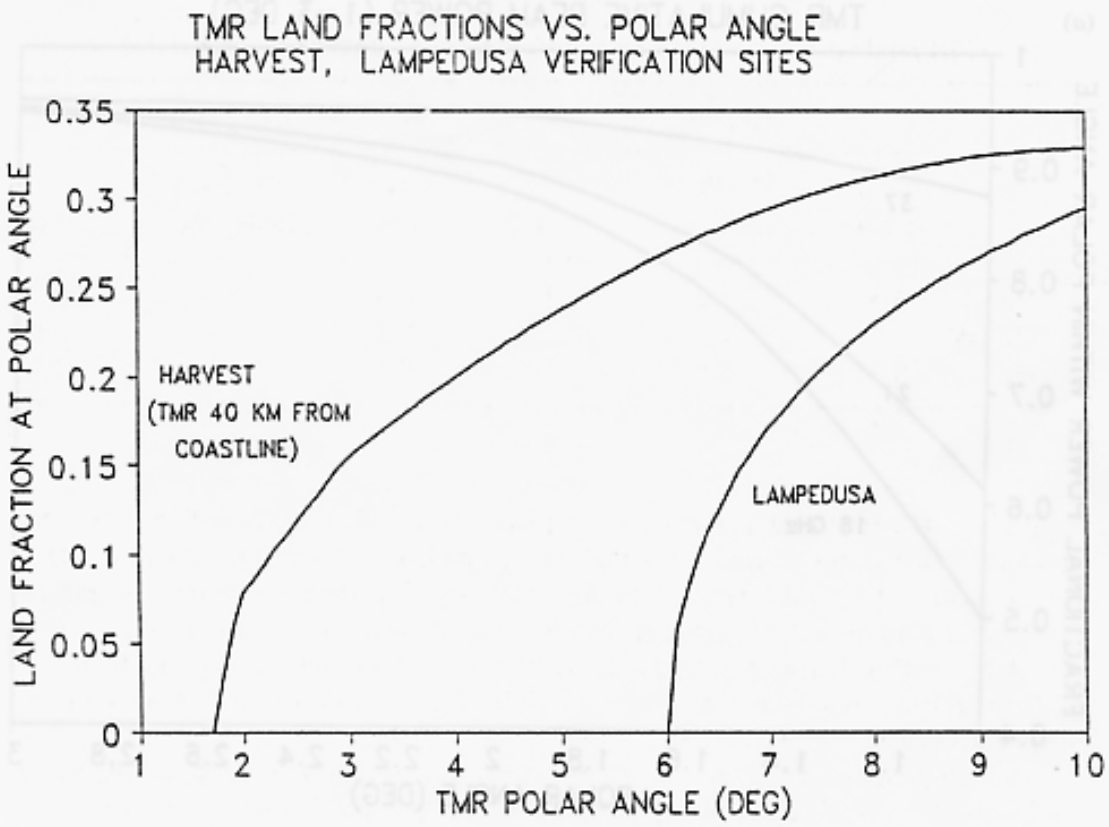

Figure 4. Land fractions within the TMR main beam vs. polar angle at the Harvest and Lampedusa verification sites. At Harvest the TMR groundtrack location for comparisons with the WVR data is chosen to be 40 km from the California coastline (~30 km from the Harvest platform).

The computed results for the main beam, on-Earth side lobe, and total land contamination effects at Harvest and Lampedusa are shown in Table 2. The largest effects are in the 18- and 21-GHz channels at Harvest for which the largest fraction of the main beam covers land. At Lampedusa, which lies ~140 km from Tunisia, the perturbation is dominated by the on-Earth side lobe effects and the fact that ~80% of the 10–55° beam views land. The uncertainty of the Harvest and Lampedusa land contamination corrections is estimated to be $< 20\%$ of the computed values based on 10-K variability in land brightness temperature, 10% uncertainty in land fraction estimates, and 15% uncertainty in the on-Earth side lobe fraction $F_{10\text{-}55}$. The largest uncertainties are for the 18- and 21-GHz channels at Harvest where the largest fractions of the main beam view land. The reason why the highest residual offsets at all three TMR frequencies occur at the Lampedusa site is not clear. One possible explanation is an error in the on-Earth side lobe fractions, which would affect the Lampedusa land correction approximately twice as strongly as at Harvest.

The land-corrected TMR brightness temperature "offsets," relative to the WVR predictions at the overpass sites, are obtained by subtracting the total land effects in Table 2 from the measured offsets shown in Figure 2. The results are given in Table 3, including the Norfolk comparison data for which no land correction was applied. (Note that the relatively high beam efficiencies allow us to assume that the computed land effects are equivalent for antenna and brightness temperatures.) The result is an apparent 1- to 2-K enhancement relative to the WVR predictions which may be due to a slightly higher calm

Table 2
TMR land contamination effects at Harvest and Lampedusa (in Kelvin)

	Harvest			Lampedusa		
	Main beam	On-Earth side lobes	Total	Main beam	On-Earth side lobes	Total
18 GHz	2.5	1.2	3.7	0.2	2.0	2.2
21 GHz	1.8	1.1	2.9	0.2	1.8	2.0
37 GHz	0.8	0.9	1.7	0.2	1.5	1.7

sea surface flux than that predicted for a plane layer with the Klein–Swift dielectric properties. This result is also supported by comparisons of the final algorithm TMR measurements with model predictions for cold, dry, high-latitude regions, where the measured brightness temperatures are dominated by the sea surface flux. Evidence exists that either small-scale roughness (Gaydanskiy et al., 1988) or uncertainties in the Klein–Swift dielectric property model above 10 GHz (Wentz, 1992) could account for the measured offsets.

The reliability of the 1- to 2-K enhancement result depends primarily on the uncertainties of the final TMR calibration algorithms. If the entire 10% scale error in the original TMR–radiosonde path delay comparisons was corrected by a 10% adjustment to the retrieval algorithm's vapor absorption model, then the apparent 1- to 2-K offset between the Klein–Swift and TMR-inferred calm sea surface flux would not occur. However, based on the considerations described in the previous section, the available constraints suggest that approximately half of the scale error is due to the preflight APC gain errors. The critical element in this argument is the validity of the TMR–SSM/I comparison at the high end (~280 K) of the calibration scale. The SSM/I predictions, which led to ~6-K increases in the high-end TMR calibration, are based on data with estimated 3-K accuracy (Hollinger et al., 1990). The SSM/I accuracy combined with the uncertainties of all constraints which determined the final calibration lead to an absolute TMR brightness temperature accuracy estimate of 1.5 K (Ruf et al., 1994). This value is comparable to the proposed 1- to 2-K sea surface flux enhancement and indicates marginal

Table 3
Net brightness temperature offsets

Brightness (GHz)	Corrected TMR − WVR-predicted (K)		
	Harvest	Lampedusa	Norfolk
18	0.2	1.9	1.4
21	1.1	3.0	1.4
37	1.7	2.1	1.9

validity. Until further data are available, we conclude that the TMR data support a calm sea surface flux model with a 1.5-K increase relative to Klein–Swift and with 1.5-K uncertainty.

Results of TMR–WVR Path Delay Comparisons

The first full year of TMR–WVR overpass path delay retrieval comparisons are shown in Figure 5 for Harvest, Lampedusa, Norfolk, and Chichi Jima. The final TMR calibration algorithms have been used, and the WVR retrieval algorithms have been modified to reflect the 5% decrease in the vapor absorption model line strength incorporated into the TMR algorithm. With the exception of two unexplained outliers at Harvest, all data are shown, including high-wind and cloudy cases. Most of the biases seen at Harvest and Lampedusa can be explained by the land contamination effects, which have not been removed from the TMR data for these comparisons. The largest bias, ~1 cm at Lampedusa, is consistent with the 0.9-K relative offset (Figures 2a,b) between the 21- and 18-GHz channels at Lampedusa. It is noteworthy that when the land contamination corrections are applied at Harvest and Lampedusa, the rms residuals at all sites are less than 1 cm of path delay difference, well within the mission specification accuracy of 1.2 cm.

The scatter at all sites is remarkably low, especially when the effects of WVR and spatial decorrelation errors are taken into account. This result illustrates an important

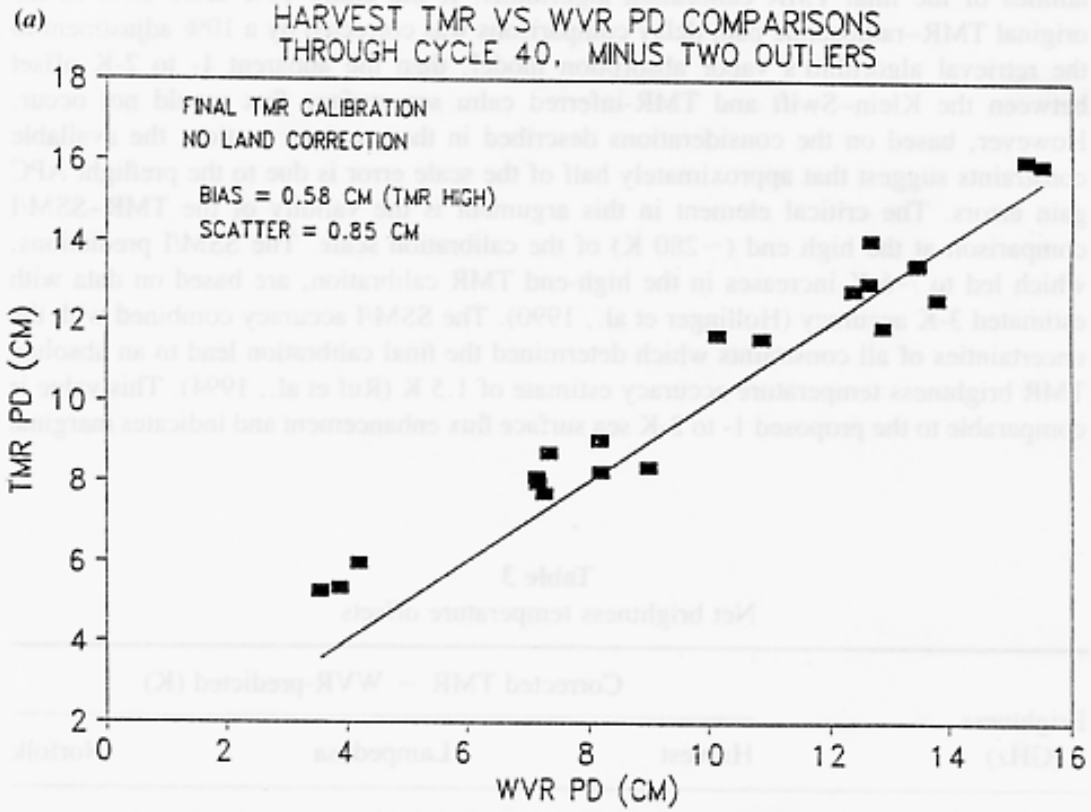

Figure 5. Harvest (a), Lampedusa (b), and Norfolk–Chichi Jima (c) overpass comparisons of TMR-retrieved and WVR-retrieved path delay for data through cycle 40, including cloudy and windy cases. The final TMR calibration algorithms have been utilized, but no land correction applied.

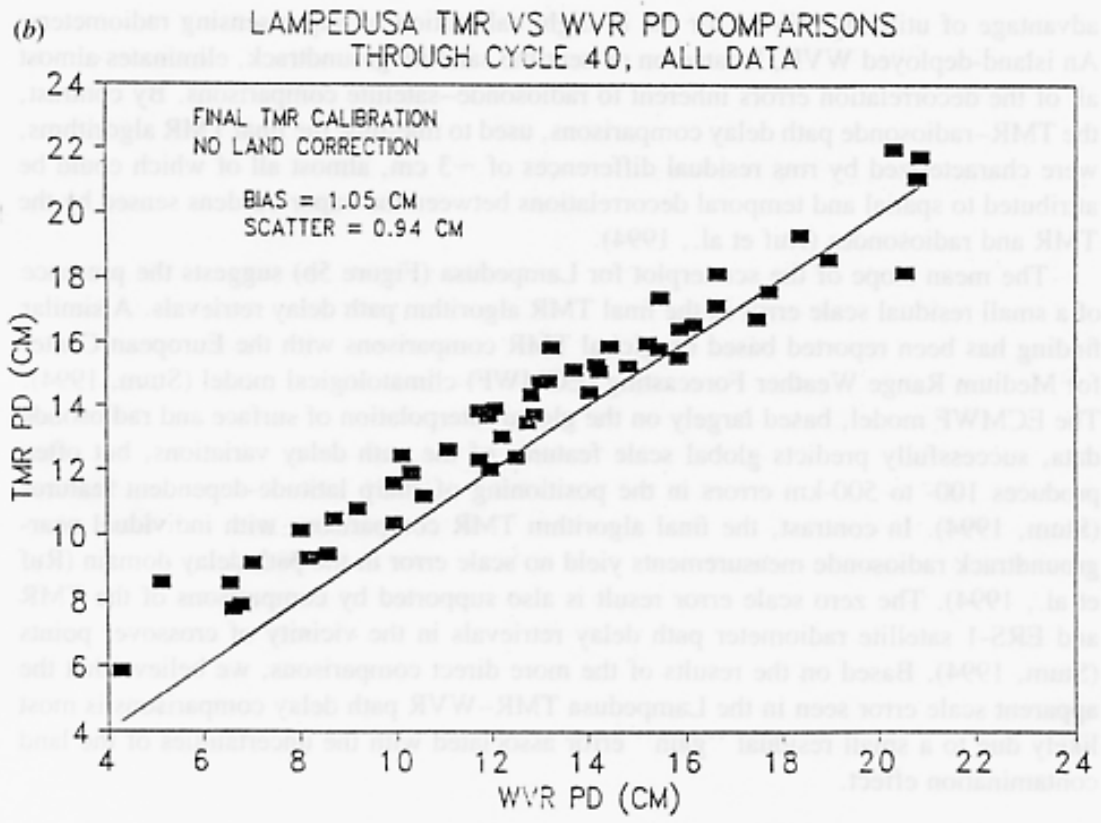

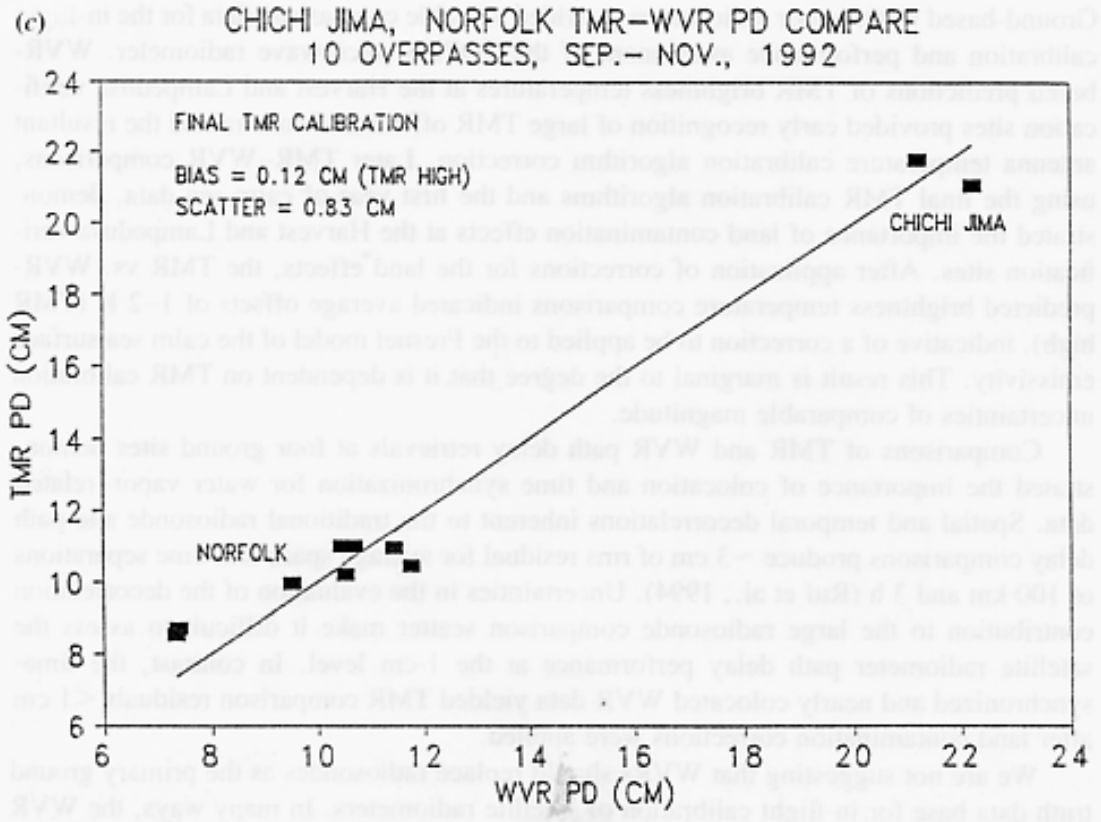

Figure 5. (*Continued*)

advantage of utilizing WVRs for the in-flight calibration of vapor-sensing radiometers. An island-deployed WVR, located on or near the satellite groundtrack, eliminates almost all of the decorrelation errors inherent to radiosonde–satellite comparisons. By contrast, the TMR–radiosonde path delay comparisons, used to fine-tune the final TMR algorithms, were characterized by rms residual differences of ~3 cm, almost all of which could be attributed to spatial and temporal decorrelations between the vapor burdens sensed by the TMR and radiosondes (Ruf et al., 1994).

The mean slope of the scatterplot for Lampedusa (Figure 5b) suggests the presence of a small residual scale error in the final TMR algorithm path delay retrievals. A similar finding has been reported based on global TMR comparisons with the European Center for Medium Range Weather Forecasting (ECMWF) climatological model (Stum, 1994). The ECMWF model, based largely on the global interpolation of surface and radiosonde data, successfully predicts global scale features of the path delay variations, but often produces 100- to 500-km errors in the positioning of sharp latitude-dependent features (Stum, 1994). In contrast, the final algorithm TMR comparisons with individual near-groundtrack radiosonde measurements yield no scale error in the path delay domain (Ruf et al., 1994). The zero scale error result is also supported by comparisons of the TMR and ERS-1 satellite radiometer path delay retrievals in the vicinity of crossover points (Stum, 1994). Based on the results of the more direct comparisons, we believe that the apparent scale error seen in the Lampedusa TMR–WVR path delay comparisons is most likely due to a small residual "gain" error associated with the uncertainties of the land contamination effect.

Summary and Discussion

Ground-based water vapor radiometers provided valuable comparison data for the in-flight calibration and performance assessment of the TOPEX microwave radiometer. WVR-based predictions of TMR brightness temperatures at the Harvest and Lampedusa verification sites provided early recognition of large TMR offsets and constrained the resultant antenna temperature calibration algorithm correction. Later TMR–WVR comparisons, using the final TMR calibration algorithms and the first year of calm sea data, demonstrated the importance of land contamination effects at the Harvest and Lampedusa verification sites. After application of corrections for the land effects, the TMR vs. WVR-predicted brightness temperature comparisons indicated average offsets of 1–2 K (TMR high), indicative of a correction to be applied to the Fresnel model of the calm sea surface emissivity. This result is marginal to the degree that it is dependent on TMR calibration uncertainties of comparable magnitude.

Comparisons of TMR and WVR path delay retrievals at four ground sites demonstrated the importance of colocation and time synchronization for water vapor–related data. Spatial and temporal decorrelations inherent to the traditional radiosonde site path delay comparisons produce ~3 cm of rms residual for average space and time separations of 100 km and 3 h (Ruf et al., 1994). Uncertainties in the evaluation of the decorrelation contribution to the large radiosonde comparison scatter make it difficult to assess the satellite radiometer path delay performance at the 1-cm level. In contrast, the time-synchronized and nearly colocated WVR data yielded TMR comparison residuals <1 cm after land contamination corrections were applied.

We are not suggesting that WVRs should replace radiosondes as the primary ground truth data base for in-flight calibration of satellite radiometers. In many ways, the WVR and radiosonde data are complimentary. The radiosonde stations rapidly provide a large

global data base which constrains biases and scale errors in the water vapor–related satellite radiometer retrievals. For vapor-induced path delay, the radiosonde measurements are direct, not requiring a model-dependent conversion from measured brightness temperatures. WVRs are most useful for the satellite radiometer brightness temperature calibration and instrument performance monitoring. The direct measurement of sky brightness temperatures at or near the satellite radiometer frequencies provides an accurate (0.5 K) constraint on the highly variable atmospheric contributions to the downward-viewing instrument. The addition of a well-constrained calm sea surface flux component to the WVR measurements then allows direct comparisons in the brightness temperature domain, yielding satellite radiometer calibration accuracies at the 1- to 2-K level.

For future altimetry satellite missions which include a microwave radiometer to provide the tropospheric range correction, it is recommended that one WVR be included to supplement the standard global radiosonde comparisons in the in-flight verification plan. The ideal deployment location would be a small island radiosonde station, at least 500 km from the nearest large land mass, and within 50 km of a midlatitude node-crossing position of the satellite groundtrack. As demonstrated by the WVR performance at Lampedusa, the instrument could operate in an unattended mode for a year or more, with data transfer via modem or monthly downloading by radiosonde station personnel. The required on-site manpower support is minimal, consisting mainly of preoverflight checks, which include cleaning of the WVR radome and reflector surfaces. Deployment at a radiosonde weather station would also provide useful support data such as cloud cover, wind speed, and comparisons to monitor the WVR performance.

Other desirable characteristics of the deployment site would include a high percentage of low-wind and cloud-free conditions and large seasonal variations in vapor abundance. Calm and clear conditions minimize comparison uncertainties associated with wind-induced emissivity variations and horizontal variations in the cloud effects. The seasonal variations determine the dynamic range over which the instrument calibration and retrieval performance can be monitored. Radiosonde statistics from candidate island weather stations would be analyzed to find a site which best satisfies the above criteria.

References

Alishouse, J. C., S. A. Snyder, J. Vongsathorn, and R. R. Ferraro. 1990. Determination of oceanic total precipitable water from the SSM/I. *IEEE Trans. Geosci. Rem. Sensing* 28: 811–816.

Becker, G. E., and S. H. Autler. Water vapor absorption of electromagnetic radiation in the centimeter wavelength range, *Phys. Rev.* 70: 300–307.

Carlisle, G., A. Dicicco, H. M. Harris, A. Salama, and M. Vincent. 1991. TOPEX/Poseidon Project Mission Plan, Jet Propulsion Laboratory, Pasadena, CA, Document No. D-6862, Rev. B.

Gaydanskiy, S. I., V. Y. Gershenzon, and V. K. Gromov. 1988. Detection of surface manifestations of internal waves in the ocean by microwave radiometry, *Izvestiya, Atmos. Ocean. Phys.* 24: 731–735.

Hill, R. J. 1986. Water vapor-absorption line shape comparison using the 22-GHz line: The Van Vleck-Weisskopf shape affirmed, *Rad. Sci.* 21: 447–451.

Hollinger, J. P., J. L. Pierce, and G. A. Poe. 1990. SSM/I instrument evaluation, *IEEE Trans. Geosci. Rem. Sensing* 28: 781–790.

Janssen, M. A., C. S. Ruf, and S.J. Keihm. 1995. TOPEX/Poseidon microwave radiometer (TMR): II. Antenna pattern correction and brightness temperature algorithm. *IEEE Trans. Geosci. Rem. Sensing* (in press).

Keihm, S. J. 1991. Water vapor radiometer intercomparison experiment: Platteville, Colorado, March 1–14, 1991. Final report prepared for Battelle, Pacific Northwest Laboratories on behalf of the Department of Energy. Jet Propulsion Laboratory Doc. No. D-8898.

Keihm, S. J. 1992. Atmospheric absorption from 20-32 GHz: Radiometric constraints on the vapor and oxygen components. *Proc. of Specialists Meeting on Microwave Radiometry and Remote Sensing Applications*, E. R. Westwater, ed. Boulder, Colorado, pp. 211–218.

Keihm, S. J., M. A. Janssen, and C. S. Ruf. 1995. TOPEX/Poseidon microwave radiometer (TMR): III. Wet troposphere range correction algorithm and pre-launch error budget. *IEEE Trans. Geosci. Rem. Sensing* (in press).

Klein, L. A., and C. T. Swift. 1977. An improved model for the dielectric constant of sea water at microwave frequencies. *IEEE J. Oceanic Eng.* OE-2: 104–111.

Lipes, R. G. 1982. Description of SEASAT Radiometer status and results. *Journal of Geophysical Research* 87: 3385–3395.

Ruf, C. S., S. J. Keihm, and M. A. Janssen. 1995. TOPEX/Poseidon microwave radiometer (TMR): I. Instrument description and antenna temperature calibration. *IEEE Trans. Geosci. Rem. Sensing* (in press).

Ruf, C. S., S. J. Keihm, B. Subramanya, and M. A. Janssen. 1994. TOPEX/Poseidon microwave radiometer performance and in-flight calibration. *Journal of Geophysical Research*. 99: 24915–24926.

Schwartz, B. E., and C. A. Doswell III. 1991. North American rawinsonde observations: Problems, concerns, and a call to action. *Bulletin of the American Meteorological Society* 72: 1885–1896.

Stum, J. 1994. A comparison between TOPEX microwave radiometer, ERS-1 Microwave Radiometer and ECMWF derived wet tropospheric corrections. *Journal of Geophysical Research*. 99: 24927–24939.

Wentz, F. J. 1992. Measurement of oceanic wind vector using satellite microwave radiometers. *IEEE Trans. Geosci. Rem. Sensing*. 30: 960–972.